FOCUS ISSUE

Check for updates

Exploring the limits of Fe^{3+} solid solution in calcium hexaluminate

P. G. de la Iglesia[1], O. García-Moreno[2], J. L. Menéndez[1], R. Torrecillas[1], J. F. Marco[3,a)] (iD)

[1] *Centro de Investigación en Nanomateriales y Nanotecnología, Consejo Superior de Investigaciones Científicas (CSIC)-Universidad de Oviedo (UO)-Principado de Asturias, Avenida de La Vega, 4-6, 33940 El Entrego, San Martín del Rey Aurelio, Asturias, Spain*
[2] *Departamento de Geología, Universidad de Oviedo, C. Jesús Arias de Velasco, S/N, 33005 Oviedo, Asturias, Spain*
[3] *Instituto de Química Física "Rocasolano", CSIC, c/ Serrano 119, 28006 Madrid, Spain*
a) Address all correspondence to this author. e-mail: jfmarco@iqfr.csic.es

Calcium hexaluminate (CA6) forms a broad range of solid solutions by substitution of Al^{3+} with other cations such as, for example, Fe, Co, Mn, etc. Solid solutions of CA6 with magnetic ions have attracted interest because they allow designing the magnetic behavior depending on the composition of each solid solution. In this paper, we have studied materials pertaining to an area of the $CaO–Al_2O_3–Fe_2O_3$ ternary phase diagram that is potentially interesting, but which has not been too much explored so far. We report on various synthesis methods of calcium hexaluminate with iron in solid solution. The percentages of iron introduced have been varied in order to determine the maximum percentage of iron that can enter into solid solution in the calcium hexaluminate such that the materials obtained exhibit magnetic behavior.

Introduction

Calcium hexaluminate ($CaAl_{12}O_{19}$), or hibonite mineral, crystallizes in the hexagonal system with a space group $P6_3/mmc$. It has a magnetoplumbite ($PbFe_{12}O_{19}$) structure type consisting of spinel blocks and hexagonal layers. The Al^{3+} cations are distributed in five non-equivalent interstitial positions, three in octahedral coordination, one in tetrahedral coordination, and one in trigonal bipyramidal coordination [1]. Due to this structure, a wide range of solid solutions with different cations having different charges can be formed, making this compound very versatile. Calcium hexaluminate (CA6) actually forms a broad range of solid solutions (CA6ss) where the mechanism is the substitution of Al^{3+} by M^{2+}, M^{3+} or M^{4+}, where M may be Fe, Co, Mn, etc. Mn^{4+} has been introduced in CA6 causing luminescence activity [2]. Fe^{3+}, Ni^{2+}, Co^{2+}, and Sn^{4+} have been used in CA6 to produce different colors in ceramic materials, which has allowed using this compound as an inorganic pigment in the fabrication of glazes and unglazed porcelain stoneware for wall and floor tiles [3, 4]. Also, Ni- and Ti-CA6 solid solutions produced modifications in the materials impedance at high frequencies [5–7].

Solid solutions of CA6 with magnetic ions have sparked interest because they allow designing the magnetic behavior (saturation magnetization, magnetocrystalline anisotropy, microwave absorption, etc.) depending on the composition of each solid solution [8].

Pure CA6 is diamagnetic. However, in materials with high Fe_2O_3 content, a gradual growth of the magnetic susceptibility to the limit of solid solution is expected [6]. Previous works have introduced Fe^{3+} in calcium hexaluminate solid solution, studying both the phases present with increasing percentage of introduced iron and the variation of their microstructures (grain size and shape) [9]. In particular, if the suitable addition of Fe^{3+} replacing Al^{3+} in the crystal structure confers certain ferromagnetic properties [8], it would allow the production of materials with tuned magnetic properties. Thus, in case of obtaining a ferromagnetic compound, its behavior could be designed by the controlled addition of Fe^{3+} ions, which would modify both the magnetic moment and also its behavior in the microwave range. This would give new applications for this compound, such as absorbent material, phase shifting, etc. In order to achieve this goal, it is necessary to explore the limits of the solid solution of iron in CA6 within the ternary phase diagram
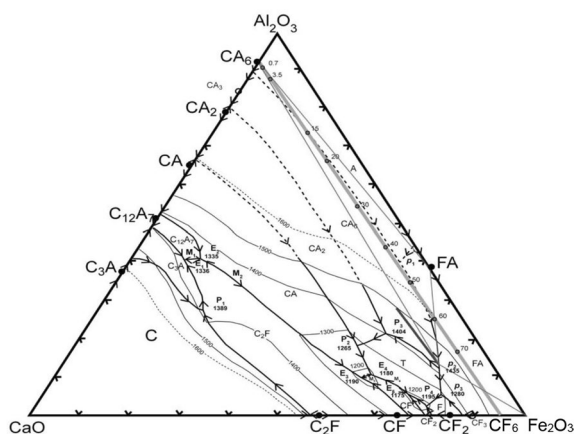
Figure 1: Ternary phase diagram $CaO-Al_2O_3-Fe_2O_3$. The compatibility triangles for the $Al_2O_3-Fe_2O_3$ side of the diagram are marked, together with the hypothetical solid solution line for CA6-(CF6) [9].

$CaO-Al_2O_3-Fe_2O_3$ (Fig. 1). The possible broad solid solution range of iron in hibonite is marked in the ternary diagram of Fig. 1 by the line connecting CA6 with the CF6 extreme in the $CaO-Fe_2O_3$ line. This peculiar solid solution with (a) wide primary crystallization field in the ternary; (b) low solubility of iron-bearing slags; and (c) stability in reducing atmospheres makes this compound an attractive refractory for the iron and steel industries [9].

The $CaO-Al_2O_3-Fe_2O_3$ ternary system has been thoroughly studied due to its relevance in Portland cement clinker production. This interest is primarily due to the fact that the calcium aluminoferrite phase is one of the four main mineralogical compounds of regular Portland cement [10].

Dealing with the solid solution of iron in hibonite, on the CA6-(CF6) line in the ternary diagram the possible solid solution of Fe^{3+} explored by [8, 9], could give place to the formation of ferromagnetic phases. In the present work, we aim to explore the mechanisms of iron solid solution in CA6 in the compositions between 20 and 70 wt% Fe_2O_3 in CA6 using different synthesis methods. We pay special attention to the characterization of the formed iron compounds to confine the limits of the solid solution to be able to interpret the obtained results.

Results and discussion

In the synthesis carried out by conventional heating of oxides mixture, previously studied by [9], a final temperature of 1400 °C was chosen for the heat treatment, with a heating rate of 5 °C/min and a dwell time of 5 h for all Fe_2O_3 percentages: 20, 30, 40, 50, 60, and 70 wt%. Figure 2 shows the XRD (CuK_α) results obtained for all the samples.

As seen in the diffraction patterns in Fig. 2(a), for 20, 30, and 40 wt% Fe_2O_3, only the diffraction peaks characteristic of
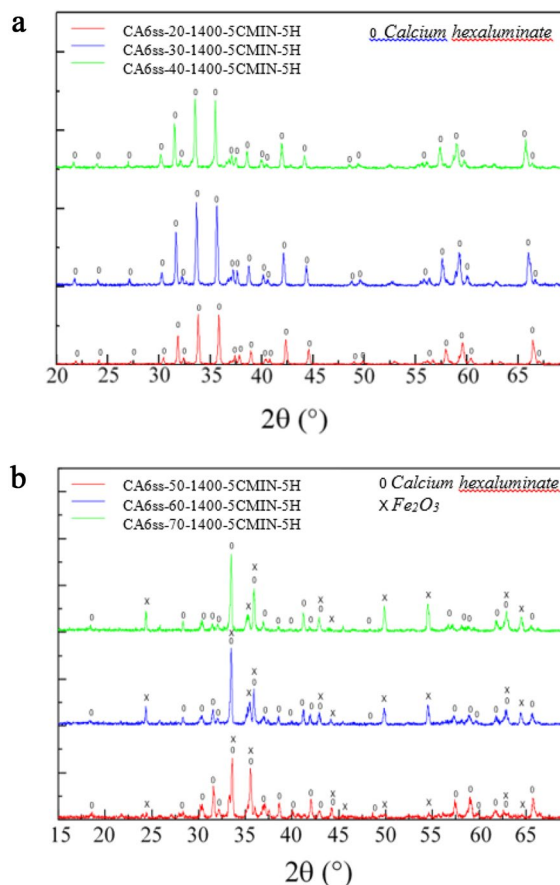

Figure 2: XRD patterns recorded using Cu K_α radiation from the materials made by mixing oxides containing different iron concentrations and heated at 1400 °C: (a) CA6ss-20 (red), 30 (blue), 4 (green)—1400 °C–5 °C/min—5 h; (b) CA6ss-50 (red), 60 (blue), 70 (green)—1400 °C–5 °C/min—5 h.

CA6ss is present. The absence of extra diffraction peaks would suggest that all the iron enters the crystal structure of calcium hexaluminate. As the iron concentration increases, the diffraction peaks shift towards lower angles. This is because Fe^{3+} has a greater ionic radius (0.64 Å) than Al^{3+} (0.50 Å), and those atoms contribute to a deformed calcium hexaluminate structure.

The Rietveld quantification for each phase is shown in Table 1. Inspection of Fig. 2(b) and Table 1 clearly indicates that increasing the initial Fe_2O_3 concentration above 40 wt%

TABLE 1: Relative concentrations of CA6ss and Fe_2O_3 obtained from the Rietveld quantification of XRD (CuK_α) measurements.

Sample	Wt% CA6ss $(CaAl_{12-x}Fe_xO_{19}) \pm 3\%$	Wt% $Fe_2O_3 \pm 3\%$
CA6ss-40	100	0
CA6ss-50	80.6	19.4
CA6ss-60	73.2	26.8
CA6ss-70	57.3	42.7

increases the amount of Fe_2O_3 as free phase in the final product. This means that in these experiments, not all the iron can be introduced in the CA6 crystal structure when the initial amount of Fe_2O_3 is over 40 wt%, which is in agreement with that observed in previous studies [9] but contrast with some more recent studies which claim to have introduced up to 53% [11] or even 57% [12] wt.% Fe_2O_3. The phase relations seem, however, to be simplified in our experiments, where only CA6ss and Fe_2O_3 have been identified, compared with the more complex phase assemblage found in [9].

In view of the XRD results in this set of samples, we selected two of them (40 and 50 wt% Fe_2O_3) for their characterization by Mössbauer spectroscopy since this technique allows a more precise qualitative and quantitative characterization of iron-containing phases. The corresponding spectra are shown in Fig. 3.

Both Mössbauer spectra exhibit a magnetic component with parameters (Table SI1) characteristic of α-Fe_2O_3. The relative spectral area corresponding to α-Fe_2O_3 is 19% for sample CA6ss-40 and 38% for sample CA6ss-50. The spectra also contain two paramagnetic doublets which can be associated with hibonite. Although the spectrum of hibonite has been usually fitted to three doublets [1] (each one corresponding to the tetra-, penta- and octahedral Fe^{3+} ions in its structure), we used here a simplified approach since we recorded the data in a wide range

of velocities (as we wanted to check the formation of α-Fe_2O_3) and we lack of resolution in the central part of the data. Therefore, we used just two doublets to fit the paramagnetic part of the spectrum. The most intense one has Mössbauer parameters (Table SI1) intermediate between these characteristics of 4- and 6-folded Fe^{3+} and, therefore, originates from the tetrahedral and octahedral Fe^{3+} in the hibonite structure. The Mössbauer parameters of the less intense doublet (Table SI1) are associated with the pentacoordinated bipyramidal trigonal Fe^{3+} site which is characterized by a very large quadrupole splitting (2.46–2.48 mms^{-1}) given its very distorted character. It is interesting to note that Mössbauer spectroscopy has identified the presence of α-Fe_2O_3 in the CA6ss-40 sample while it went undetected in the XRD measurements. It also identified a larger amount of α-Fe_2O_3 in the CA6ss-40 than that found by XRD. This confirms the ability of Mössbauer spectroscopy to identify iron-containing phases when compared with XRD diffraction using Cu K$_\alpha$ radiation. Summarizing, the results indicate that these materials are composed by hematite and a hibonite phase.

The results shown in Fig. 3 reveal that there is not only a pure CA6ss phase formed for the starting 40 wt% Fe_2O_3, so that the limit of iron solid solution for these experimental conditions is, in fact, smaller than 40%, being closer to a 35% and, hence, according to a formulation such as $CaAl_{8.7}Fe_{3.3}O_{19}$ (this calculation assumes equal recoil free fractions for hematite and iron hibonite).

It has been reported [11] that iron hibonites of composition $CaAl_9Fe_3O_{19}$ are paramagnetic in the temperature range 5–350 K while $CaAl_8Fe4O_{19}$ has a Curie temperature of 130 K. Therefore, the hysteresis loop observed in the present samples see (Fig. 1 in the Supplementary Information) has to be related with the presence of α-Fe_2O_3 [12]. It is known that hematite is weakly ferromagnetic due to the occurrence of spin canting and hysteresis loops have been recorded from hematite samples since very long (see [13] and references therein), the values of the coercive field and saturation depending on the characteristics of the sample (particle size, occurrence of strain, etc.).

As stated above, and in order to test if the use of different synthesis methods could influence the amount of iron entering the CA6ss, we decided to study other methods of finer synthesis and reagents that could provide powders with more homogeneous compositions. The first of those methods tested was the Organic Steric Entrapment Method (OSEM).

Under the light of the previous results, the compositions synthetized by this method were focused on the Fe_2O_3 content interval from 40 to 60 wt%. The preparation temperatures for the OSEM samples were 1250, 1300, 1350, and 1400 °C. The results of these heat treatments showed that at 1250 °C, a very small amount of CA6ss is formed. Opposite to this, at 1400 °C, samples are partially fused. Therefore, we selected for characterization those samples treated at temperatures of 1300 and
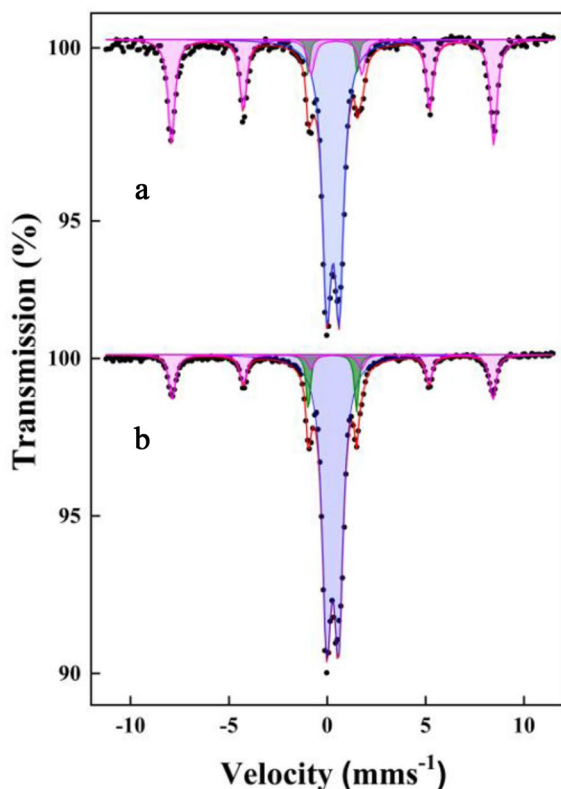
Figure 3: Mössbauer spectra recorded at room temperature from the oxide-mixed samples (a) CA6ss-50-1400 °C; (b) CA6ss-40-1400 °C.

1350 °C. We used a heating rate of 5 °C/min and a dwell time of 15 h. In this case, XRD was performed using MoK_α radiation in order to obtain a better phase identification avoiding α-Fe_2O_3 masking with the CuK_α radiation. Diffractograms for the heat-treated samples with initial 40, 50, and 60 wt% Fe_2O_3 content (CA6ssOSEM-40, -50, and -60, respectively) at 1300 and 1350 °C, are shown in Fig. 4.

The diffractograms recorded from these materials resulted to be very complex. They contain a large number of peaks and, particularly in the samples containing 40 and 50 wt% Fe_2O_3 (both in the 1300 °C and 1350 °C materials), there is an evident broadening of the diffractions signals suggesting the occurrence of amorphous/small grain-sized components. The diffraction peaks are displaced to the left in the diffractogram with increasing starting iron content in the samples, indicating that a greater amount of iron is introduced in the CA6 structure. Sample CA6ssOSEM-40 presents only peaks that correspond to a CA6 solid solution. For higher initial Fe_2O_3 contents, peaks of other compounds (α-Fe_2O_3 and hercynite) are present in the diffractograms. The presence of hercynite is considerably large in the CA6ss-OSEM-60 samples due to the high concentration of iron that does not enter into the solid solution.
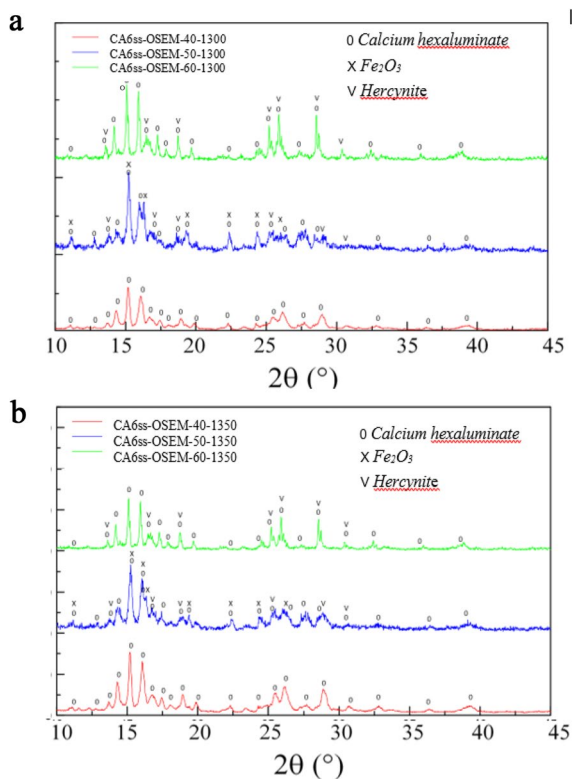

Figure 5: Mössbauer spectra recorded at room temperature from the OSEM samples: (a) CA6ss-OSEM-50 at 1350 °C; (b) CA6ss-OSEM-50 at 1300 °C; (c) CA6ss-OSEM-60 at 1350 °C; and (d) CA6ss-OSEM-60 at 1300 °C.

Figure 4: XRD patterns recorded using MoK_α radiation from the OSEM materials heated at (a) 1300 °C, samples CA6ss-OSEM-40 (red), -50 (blue), 60 (green)—1300-5cmin-15 h; and (b) 1350 °C, samples CA6ss-OSEM-40 (red), 50 (blue), 60 (green)—1350-5cmin-15 h.
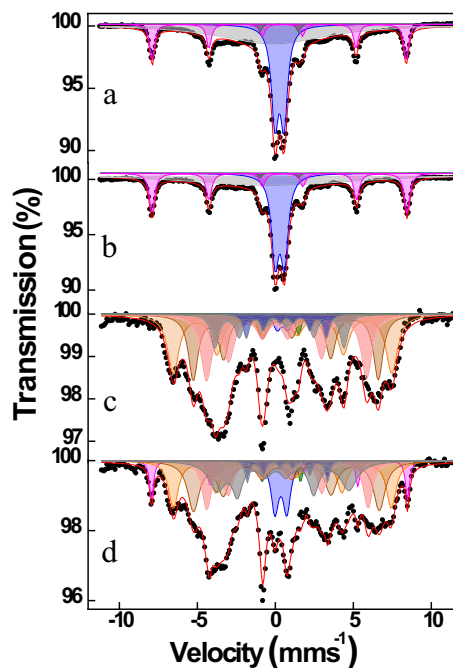
Mössbauer spectroscopy phase analysis (Fig. 5) was performed for samples CA6ss-OSEM-50 and -60 (1300 °C and 1350 °C) as they showed greater complexity in the phase assemblages. So, the Mössbauer spectra recorded from the samples CA6ss-OSEM-50-1300 °C and CA6ss-OSEM-50-1350 °C were relatively simple and similar to those recorded from sample CA6ss-50%-1400 °C.

They were composed (see Table SI2 in SI) by a magnetic sextet characteristic of hematite, a paramagnetic part typical of Fe^{3+} in the hibonite structure and a very broad, unresolved magnetic component which is of difficult assignment and is usually associated to the presence of systems displaying strong magnetic relaxation due to small size grains or diluted magnetic interactions. This component could be related to the phases which give place to the broadening of the diffractograms shown in Fig. 4.

On the contrary, the spectra recorded from CA6ss-OSEM-60-1300 °C and CA6ss-OSEM-60-1350 °C showed a tremendous complexity (Fig. 5). They showed a very complicated, asymmetric magnetic pattern arising from the superposition of various magnetic sextets with very different isomer shifts, quadrupole shifts, and hyperfine magnetic fields. Inspection of the central part of the spectra indicated the occurrence of paramagnetic contributions which can be associated to an iron hibonite phase. Obviously, various plausible fitting models can be tried, but there is no one which can give a definitive answer. Hence, we adopted a systematic model, which

included between 5 and 6 magnetic components depending on the sample (see Fig. 5 and Table SI2). There are a few conclusions that can be extracted from these data. The first one is that while CA6ss-OSEM-60-1300 °C contains a hematite contribution (the presence of a component with a hyperfine magnetic field of around 50.9 T well separated from the rest of the spectrum is clearly resolved) this is not the case of sample CA6ss-OSEM-60-1350 °C. In the spectrum of this sample, the maximum hyperfine magnetic field is located at around 43.4 T. A component having such a value is also observed in the spectrum of sample CA6ss-OSEM-60-1300 °C. These contributions might be due, in view of the XRD results, to the presence of some type of hercynite or iron-aluminum spinel. In an early paper, Dehe et al. [14] studied the spinel system $Fe_{3-x}Al_xO_4$ with $0 \leq x \leq 1.05$ They found that for $x \geq 0.9$ the corresponding spectra only showed paramagnetic components, while for $x < 0.9$, they showed several Zeeman components which, depending on the x value, ranged from 39.2 T to 48.4 T and they associated these different components with different cation distributions over the octahedral and tetrahedral sites of the spinel structure. It seems plausible, then, to associate that component with the presence of a $Fe_{3-x}Al_xO_4$ spinel the value of x is uncertain. However, in the present case, the most intense contribution corresponds to components with hyperfine magnetic fields in the range 34–36 T, values which appear to be smaller than those reported in the above-mentioned paper. These components are characterized by very large quadrupole shifts what suggest that they correspond to highly distorted Fe^{3+} environments. Although it is true that due to the complexity of the data the determination of the hyperfine parameters has to be affected by a large uncertainty, these high quadrupole shifts values seem to be genuine and not a mere fitting artifact as they appear very consistently during the evaluation of the spectra. In fact, it is clear that they need to be large, otherwise the significant asymmetry of the spectra could not be reproduced by any means. The assignment of these magnetic components to particular chemical species is complicated as the corresponding XRD patterns of these samples do no result very helpful in this regard. They might probably correspond to disordered Fe–O–Al phases that went undetected by XRD. The low hyperfine magnetic fields might be related to the occurrence of disorder and/or the presence of local Al^{3+}-rich regions within the solid which would dilute the magnetic interactions between the iron ions. In any case, being these plausible interpretations, the determination of the real nature of these magnetic components is something that goes beyond of the scope of this paper. Finally, both spectra present also consistently the presence of a very minor component characterized by a large isomer shift and a low hyperfine magnetic field which suggest the presence of a phase containing some Fe^{2+} cations.

Due to the broadness of the spectra and the strong overlap of the different components, it is difficult to ascertain whether there is any paramagnetic component that could be associated to the presence of a canonical hercynite phase $FeAl_2O_4$ (or a stoichiometry able to give a paramagnetic component which could be associated to this spinel-related compound). If this was the case, the spectra should contain Fe^{2+} doublets, something that does not result evident from the spectra and that resisted fitting. Summarizing, the samples CA6ss-OSEM-50-1300 °C and CA6ss-OSEM-50-1350 °C contain hematite, hibonite, and a magnetic component that might be due to an unresolved, disordered Fe-Al spinel contribution. In these samples, the final calcination temperature does not appear to play an important role. The composition of the CA6ss-OSEM-60-1300 °C and CA6ss-OSEM-60-1350 °C is much more complex as they can plausibly contain different Fe-Al-disordered phases. In these samples, the final heating temperature plays an important role: while CA6ss-OSEM-60-1300 °C contains both hematite and hibonite contributions, CA6ss-OSEM-60-1350 °C does not show any hematite phase and only shows a very minor hibonite component.

The magnetic characterization was performed on the sample CA6ss-OSEM-40 synthetized at 1300 and 1350 °C, as the XRD using MoK_α radiation showed the presence of CA6ss single phase. The hysteresis cycles for these samples are shown in Fig. 2 of the Supplementary Information.

It is observed that in both cases, the hysteresis loops indicate the presence of a ferromagnetic material. The coercive fields are 32 and 167 Oe, respectively, and the remanence is only 7.5 and 30.5%. According to Mössbauer spectroscopy, CA6ss is paramagnetic; therefore, the observed hysteresis cycle must be due to the presence of residual phases of ferromagnetic compounds that are not detectable by XRD even using MoK_α radiation. In any case, the saturation magnetization of the CA6ss-OSEM-40-1300 °C sample is significantly lower than the corresponding one made by mixing oxides synthesis what suggests that the amount of magnetic compounds is much lower in the present case for this initial Fe_2O_3 concentration.

While the magnetic measurement results indicate that in the sample having 40 wt% Fe_2O_3, the present synthesis method might accommodate more Fe^{3+} within the hibonite structure than with the previous synthesis procedure, this is not the case in the samples having larger initial percentages of iron oxide. In the case of the CA6ss-OSEM-50 samples, the amount of iron-containing hibonite amounts to ca. 30% according to Mössbauer spectroscopy, while in the corresponding CA6ss-50 sample made by a mixture of oxides, the percentage of iron-containing hibonite is much higher (more than 60%). Although it is true that the amount of free α-Fe_2O_3 is smaller in the CA6ss-OSEM-50 samples, they show in their Mössbauer spectra an unresolved magnetic component which, therefore, cannot be related to CA6ss and that contributes with about a 50% to the total spectral area. The situation above 50 wt% initial Fe_2O_3

is much more complicated as the number of magnetic phases observed by Mössbauer spectroscopy exceeds 95% of the spectral area. This implies that beyond this initial concentration of starting Fe_2O_3, iron does not enter in significant amounts the hibonite structure but rather prefers to form a multiplicity of different magnetic iron phases.

The effect of the synthesis method used to fabricate CA6ss was also tested using the sol–gel method. With this synthesis method, samples were prepared with different percentages of initial Fe^{3+}: 40, 50 and 60 wt% Fe_2O_3, labeled CA6ssSG-40, -50 and -60, respectively.

Figure 6 shows the obtained diffractograms recorded from these samples using MoK_α radiation. The only phases present, as seen in the diffractograms at 1300 and 1350 °C, are CA6ss and Fe_2O_3. As it was observed in the previously described synthesis method (OSEM), the diffraction peaks are shifted to the left due to the changes in the structure of calcium hexaluminate with the incorporation of Fe^{3+}. Sample CA6ss-SG-40 only shows the diffraction peaks of CA6ss. The intensities of the CA6ss peaks decrease gradually for 50 and 60 wt% Fe_2O_3, which can be interpreted as being the mechanism of solid solution completed only for 40 wt% Fe_2O_3. The diffractograms also
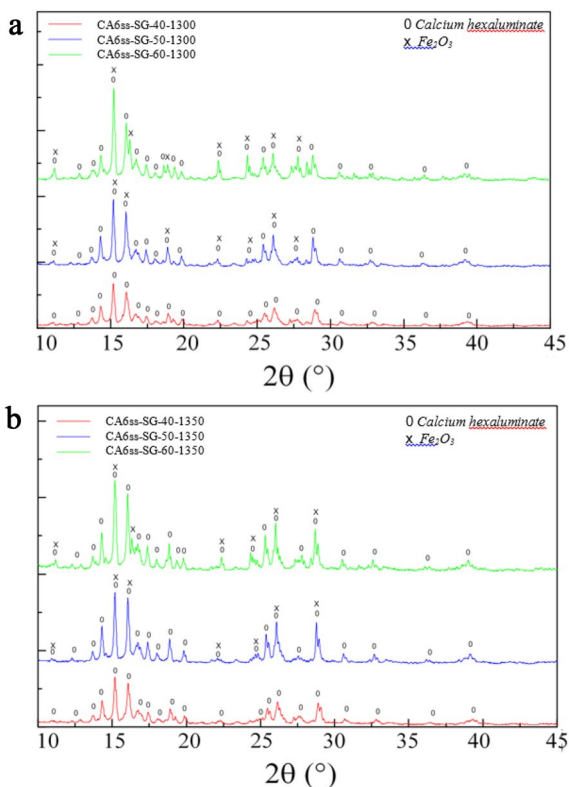

Figure 7: Mössbauer spectra recorded at room temperature from the SG samples: (a) CA6ss-SG-50 at 1350 °C; (b) CA6ss-SG-50 at 1300 °C; (c) CA6ss-SG-60 at 1350 °C; and (d) CA6ss-SG-60 at 1300 °C.

show some broadening what suggests the possibility that amorphous or poorly crystalline phases are also contributing to the final pattern.

Mössbauer results are shown in Fig. 7 for samples CA6ss-SG-50 and -60. The spectrum recorded from CA6ss-SG-50-1300 showed only the presence of hematite and hibonite (see Table SI3). The spectrum corresponding to CA6ss-SG-50-1350 showed an additional broad, relaxed, very intense magnetic component of which assignment to a particular phase is difficult. The hematite and hibonite contributions here are much smaller than in the previous sample. The spectrum recorded from CA6ss-SG-60-1300 was very similar to that of CA6ss-SG-50-1350 except for a much more intense hematite contribution. It also showed a hibonite component and, again, a broad, unresolved magnetic component. The spectrum recorded from CA6ss-SG-60-1350 was much more complex. Very similar comments to those made for the samples synthetized via the OSEM method can be applied here. In the present sample, we have too $Fe_{3-x}Al_xO_4$ contributions although, opposite to the OSEM samples, we have here more significant hematite and hibonite contributions.

The hysteresis loops recorded from sample CA6ss-SG-40 are shown in Fig. 3 of the Supplementary Information. It is observed that for both CA6ss-SG-40 samples made after heating at 1300 and 1350 °C, hysteresis loops correspond to a weakly ferromagnetic material. The coercive field in both cases is 173 and 162 Oe, respectively, and remanence is only 10.8 and 5.2%. As stated above, the presence of a residual α-Fe_2O_3 phase, not detectable

Figure 6: XRD patterns recorded using MoK_α radiation from the sol–gel materials at (a) 1300 °C, samples CA6ss-SG-40 (red), 50 (blue), 60 (green)—1300-5cmin-15 h; and (b) 1350 °C, samples CA6ss-SG-40 (red), 50 (blue), 60 (green)—1350-5cmin-15 h.
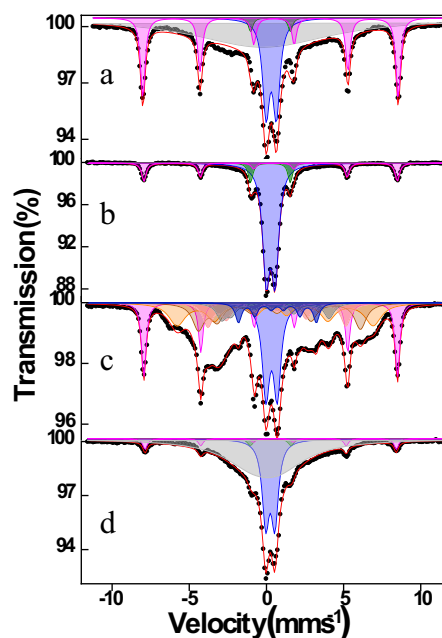
by XRD, has to be in the origin of the hysteresis loops observed here. The hysteresis loops of samples with higher iron content revealed the interaction of the several (ferromagnetic) phases present in the samples.

There are a few interesting findings in this last set of samples. One of them is that the sample CA6ss-SG-50-1300 °C contains a large percentage of hibonite (83%) what contrasts strongly with the corresponding OSEM sample. Furthermore, there is no evidence in its Mössbauer spectrum of any other magnetic phases apart for α-Fe_2O_3. This also contrasts with the sample CA6ss-50-1400 °C which shows a smaller percentage of hibonite (68%), see above. This would imply that the SG method is able to incorporate a larger amount of iron in the CA6 structure without need to heat at a higher temperature. Contrarily to the OSEM case, the Mössbauer spectra still show some significant hibonite contributions in the CA6ss-60 samples, i.e., although some other magnetic phases are formed, there is still the possibility that starting from 60 wt% ferric oxide in the precursors some trivalent iron can be accommodated in the hibonite structure. This does not occur to the same extent in the OSEM samples where the reaction paths seem to follow a different way promoting basically the formation of magnetically ordered species.

Conclusions

We have studied in this paper three different CA6ss synthesis methods with different iron contents, and we have found that the upper solid solution limit is always smaller than 40 wt% Fe_2O_3, being close to a 35% allowing to formulate the iron hibonite compounds as $CaAl_{8.7}Fe_{3.3}O_{19}$. Although iron hibonite compounds of composition $CaAl_6Fe_6O_{19}$ have been claimed to be obtained [12], the stoichiometry was deduced from XRD data and we have found in this paper that XRD fails to detect small fractions of hematite. Other authors [11] have pointed out very recently that the limit of solid solution is reached for compositions $CaAl_{6.5}Fe_{5.5}O_{19}$, their corresponding Mössbauer spectra being free of hematite components. We must mention, however that the spectra were presented in the velocity range ± 2 mms^{-1} and, consequently, they might have missed a small hematite contribution. The samples in [11] were made by calcination of a mixture of iron oxide, aluminum oxide, and calcium carbonate at temperatures between 1350 °C and 1450 °C or 12–24 h being necessary to reheat until pure phases were obtained. Oxide-mixed synthesis in our study bring different results on the phase relations obtained from the samples made after heating at 1400 °C as compared with this and other previous works, as Mössbauer spectra show the presence of free Fe_2O_3 for initial 40 wt% Fe_2O_3. The results point out how small variations in related synthesis methods can lead to quite different results.

The results obtained by the organic steric entrapment method suggest that the solid solution might be increased provided the initial concentration of Fe_2O_3 does not exceed 40%. Starting from higher ferric oxide concentrations gives place to a higher amount of magnetically ordered species and a smaller proportion of iron-containing hibonite in the Mössbauer spectra than in the case of the other two synthesis methods. The Mössbauer data also suggest that the SG method can incorporate larger amounts of Fe^{3+} in the CA6 structure using a lower temperature of 1300 °C as compared to the oxide-mixture method.

Synthesis of materials and experimental procedure

In order to investigate the limits in the iron solid solution in calcium hexaluminate, we used three different synthesis methods. These methods are conventional synthesis by oxide-mixed powders, synthesis by organic steric entrapment method, and sol–gel synthesis.

For the synthesis of CA6ss by oxide-mixed powders, we used calcium carbonate (Sigma-Aldrich), alumina (Taimei), and iron (III) oxide (Sigma-Aldrich) as precursor materials. These are mixed in an attrition mill for two hours with propanol. Then the solvent is removed in an oven for 24 h, obtaining the final mixed powder.

CA6ss powder precursors were also obtained by the organic steric entrapment method proposed in [15]. In the organic steric entrapment method, nitrate salts from ABCR: Ca $(NO_3)_2\cdot4H_2O$, $Al(NO_3)_3\cdot9H_2O$, and $Fe(NO_3)_3\cdot9H_2O$ were the cation sources for aluminum, calcium, and iron, respectively. Stoichiometric amounts were dissolved in deionized water and stirred for 1 h before the addition of the PVA (polyvynil alcohol, Sigma Aldrich) polymer solution. The 5 wt% PVA solution was made by adding 80% hydrolyzed PVA to deionized water. The proportions of the PVA to cation sources in the solution were adjusted in such a way that there were 6 times more positively charged valences from the cations than from the potentially negatively charged –(OH) functional groups of the polymer [15]. The polymeric long chains have hydroxyl groups in solution. Hence, one PVA monomer, which has one hydroxyl (OH) functional group, can be used as a unit for calculation of PVA content. The exact relative amount of PVA to cations in the solution can be calculated with reference to a monomeric unit of PVA of molecular weight/monomer = 44.4 g. Water was evaporated by continuous stirring during heating on a hot plate. The resulting gel-type precursor was completely dried after several hours at 100 °C. The dried organic/inorganic precursors in all cases were then ground and calcined at 800 °C in an air atmosphere in a box furnace. By this method, we obtain nanometer size precursors with a high specific surface, and therefore, a more reactive material is formed that can (a priori) reduce the synthesis temperature and favor the reactivity for the introduction of iron in the Ca6 structure compared to the oxide-mixed powder.

TABLE 2: Conditions for the different synthesis methods.

Synthesis method	Wt% Fe_2O_3	Heat treatment (C)
Oxide-mixed powders	20, 30, 40, 50, 60 and 70	1400
OSEM	40, 50 and 60	1300 and 1350
Sol–gel	40, 50 and 60	1300 and 1350

The improved reactivity was also tested by synthetizing CA6ss precursors using the sol–gel method. The sol–gel process is a chemical pathway which allows manufacturing amorphous and polycrystalline materials relatively easily with a high homogeneity, a high purity, and a small particle size. It is a chemical pathway that begins with the synthesis of a colloidal suspension of solid particles or clusters in a liquid (sol) and the hydrolysis and condensation of the sol to form a full solvent solid material (gel). The precursors used are $Ca(NO_3)_2 \cdot 4H_2O$ ABCR, $Al(NO_3)_3 \cdot 9H_2O$ ABCR, $Fe(NO_3)_3 \cdot 9H_2O$ ABCR, and NH_4OH solution from Sigma-Aldrich 28% v/v.

The powder precursors from the different synthesis methods were heat treated in air atmosphere at the temperatures indicated in Table 2. Specifications for each heat treatment were exposed in the results section.

The obtained CA6ss samples were ground into powder after each heat treatment to study the phase composition by XRD with a Philips X' Pert Pro diffractometer in "Bragg–Brentano" geometry using Cu K_α radiation (45 kV and 40 mA), and a 15–70 2θ range with 0.01 step size and 1 s counting time. Using Cu K_α radiation is not always satisfactory for studying samples with low (< 10%) amounts of Fe_2O_3. For this purpose, we have also used Mo K_α radiation. The quantification of the formed phases in the XRD results was estimated using the Rietveld method with the aid of the MAUD software [16].

Mössbauer spectroscopy data were recorded at room temperature using a conventional constant acceleration spectrometer and a $^{57}Co(Rh)$ source. The velocity scale was calibrated using a 6 μm thick α-Fe foil. All the isomer shifts are referred to the centroid of the spectrum of α-Fe at room temperature.

The CA6ss materials were finally characterized for their magnetic behavior using an alternative gradient field magnetometer AGM, Micro-Mag™ 2900 (Princeton Measurements Corporation) with a maximum magnetic field 0.5 T to record the corresponding hysteresis loops.

Acknowledgments

Author contributions

Conceptualization: PGI, OGM, JLM, RT, JFM. Methodology: PGI, JLM, JFM. Formal analysis and investigation: PGI, JLM, JFM. Funding acquisition: JLM, RT. Writing—original draft: PGI, OGM, JFM. Writing—review and editing: OGM, JLM, JFM.

Funding

Data availability

The datasets generated during and/or analyzed during the current study are available from the corresponding author on reasonable request.

Declarations

Conflict of interest On behalf of all authors, the corresponding author states that there is no conflict of interest.

Open Access

Supplementary Information

The online version contains supplementary material available at https://doi.org/10.1557/s43578-022-00824-7.

References

1. D. Holtstam, Iron in hibonite: a spectroscopic study. Phys. Chem. Miner. (1996). https://doi.org/10.1007/BF00202031
2. T. Murata, T. Tanoue, M. Iwasaki, K. Morinaga, T. Hase, Fluorescence properties of Mn^{4+} in $CaAl_{12}O_{19}$ compounds as red-emitting phosphor for white LED. J. Lumin. **114**(3–4), 207–212 (2005). https://doi.org/10.1016/j.jlumin.2005.01.003

3. G. Costa et al., Ni-doped hibonite ($CaAl_{12}O_{19}$): a new turquoise blue ceramic pigment. J. Eur. Ceram. Soc. **29**(13), 2671–2678 (2009). https://doi.org/10.1016/j.jeurceramsoc.2009.04.001

4. F. Bondioli, A.M. Ferrari, C. Leonelli, T. Manfredini, Syntheses of Fe_2O_3/silica red inorganic inclusion pigments for ceramic applications. Mater. Res. Bull. **33**(5), 723–729 (1998). https://doi.org/10.1016/S0025-5408(98)00047-6

5. C.S. Prakash, V.M. Nanoti, D.K. Kulkarni, G.M. Rao, Substitutional effect of magnetic behaviour in calcium hexaferrite. J. Magn. Magn. Mater. **140–144**, 2089–2090 (1995). https://doi.org/10.1016/0304-8853(94)01409-4

6. D.K. Kulkarni, C.S. Prakash, Structural and magnetic properties of $CaAl_4Fe_8O_{19}$. Mater. Sci. **17**(1), 35–39 (1994)

7. P. Singh, V.K. Babbar, A. Razdan, S.L. Srivastava, R.K. Puri, Complex permeability and permittivity, and microwave absorption studies of $Ca(CoTi)_xFe_{12-2x}O_{19}$ hexaferrite composites in X-band microwave frequencies. Mater. Sci. Eng. B **67**(3), 132–138 (1999). https://doi.org/10.1016/S0921-5107(99)00328-1

8. F.P. Glasser, F.W.D. Woodhams, R.E. Meads, W.G. Parker, A Mössbauer and ESR study of $CaO·6Al_2O_3CaO·6Fe_2O_3$ solid solutions. J. Solid State Chem. **5**(2), 255–261 (1972)

9. C. Domínguez, R. Torrecillas, Influence of Fe^{3+} on sintering and microstructural evolution of reaction sintered calcium hexaluminate. J. Eur. Ceram. Soc. **18**(9), 1373–1379 (1998). https://doi.org/10.1016/S0955-2219(98)00067-3

10. D.A. Jerebtsov, G.G. Mikhailov, Phase diagram of $CaO–Al_2O_3$ system. Ceram. Int. **27**(1), 25–28 (2001). https://doi.org/10.1016/S0272-8842(00)00037-7

11. B.A. Duell et al., Structure and electronic properties of $CaAl_{12}FeO_{19}$ hibonites. J. Solid State Chem. **291**, 121650 (2020). https://doi.org/10.1016/j.jssc.2020.121650

12. H. Nagumo, K. Watanabe, K. Kakizaki, K. Kamishima, Synthesis and magnetic properties of Fe substituted hibonite. J. Magn. Soc. Jpn. **41**(2), 20–24 (2017). https://doi.org/10.3379/msjmag.1701R001

13. Ö. Özdemir, D.J. Dunlop, Hysteresis and coercivity of hematite. J. Geophys. Res. Solid Earth **119**(4), 2582–2594 (2014). https://doi.org/10.1002/2013JB010739

14. G. Dehe, B. Seidel, K. Melzer, C. Michalk, Determination of a cation distribution model of the spinel system $Fe_{3-x}Al_xO_4$. Phys. Status Solidi A **31**(2), 439–447 (1975). https://doi.org/10.1002/pssa.2210310212

15. M.H. Nguyen, S.-J. Lee, W.M. Kriven, Synthesis of oxide powders by way of a polymeric steric entrapment precursor route. J. Mater. Res. **14**(8), 3417–3426 (1999). https://doi.org/10.1557/JMR.1999.0462

16. L. Lutterotti, Maud: a Rietveld analysis program designed for the internet and experiment integration. Acta Crystallogr. A **56**(s1), 54 (2000). https://doi.org/10.1107/S0108767300021954